ELSEVIER

Journal of Magnetism and Magnetic Materials 238 (2002) 185–199

journal of magnetism and magnetic materials

www.elsevier.com/locate/jmmm

Finite element calculations on the single-domain limit of a ferromagnetic cube—a solution to μMAG Standard Problem No. 3

Riccardo Hertel[1], Helmut Kronmüller*

Max-Planck–Institut für Metallforschung, Postfach 80 06 65, Heisenbergstrasse 1, 70506 Stuttgart, Germany

Received 11 January 1999

Abstract

Zero field states of the magnetization in a uniaxial ferromagnetic sample of cubic shape are calculated by means of micromagnetic finite element modeling. With increasing size the minimum energy arrangement changes from a single-domain configuration (flower state) to a vortex configuration. An intermediate arrangement (twisted flower state) between the flower state and the vortex state is observed. A further magnetization state resulting in the calculation is a vortex state with a singularity of the directional field of the magnetization.

This work provides our solution to the micromagnetic Standard Problem No. 3 posed by the μMAG micromagnetic modeling activity group at the National Institute of Standards and Technology (NIST).

Keywords: Computational micromagnetism; Micromagnetic standard problem; Finite element method

1. Introduction

The magnetic states of a ferromagnetic sample are characterized by the minima of the Gibbs free energy. Within the framework of micromagnetism, the directional field of the magnetization in the sample arranges such as to minimize the sum of the most relevant energy terms. Usually, the most significant contributions to the total energy of ferromagnetic materials are the magneto-crystalline anisotropy energy, the exchange energy, the Zeeman energy and the stray field energy. In this paper we only consider zero field magnetic states so that the Zeeman energy term is omitted. If the material's parameters and the shape of the sample are given, the minimum energy arrangement depends only on the size of the sample. This size dependence of the magnetic ground state is addressed in μMAG Standard Problem No. 3 which is treated in this paper.

Micromagnetic standard problems have been set up by the μMAG group at NIST in order to obtain reliable tests of numerical algorithms. Provided that independent groups report corresponding results for well-defined problems, these standard problems can be used as checks for possible errors

*Corresponding author. Tel.: +49-711-689-1910; fax: +49-711-689-1912.

E-mail addresses: hertel@mpi-halle.mpg.de (R. Hertel), kronm@physix.mpi-stuttgart.mpg.de (H. Kronmüller).

[1] Present address: Max-Planck–Institut für Mikrostrukturphysik, Weinberg 2, 06120 Halle, Germany.

0304-8853/02/$ - see front matter
PII: S0304-8853(01)00876-9

in a numerical code. The first standard problem did not lead to satisfactory results in this sense [1]. No clear consensus can be derived from the seven anonymous submissions from different groups. A detailed discussion for the possible reasons for the discrepancies in the results of Standard Problem No. 1 is difficult to give on the basis of the available data, but in general it can be said that the first standard problem represents a too complex problem for the current state of numerical micromagnetic computations. Therefore, two further standard problems have been defined, bearing the difficulties of Standard Problem No. 1 in mind.

One of these more recent standard problems is μMAG Standard Problem No. 3. The problem specification is illustrated in Fig. 1. As only zero field states of the magnetization are considered, problems concerning switching or nucleation processes and the influence of field rates are avoided. Hence, the problem is comparatively simple. Moreover, the size of the sample is small enough to rule out discretization errors.

The task of the μMAG Standard Problem No. 3 [2] consists in calculating the single-domain limit (SDL) for a ferromagnetic cube with uniaxial anisotropy. The SDL is defined here as the critical edge length at which a mostly uniform arrangement of the magnetization, the so-called flower state, and the vortex state, i.e. a strongly non-uniform configuration, are of equal energy.

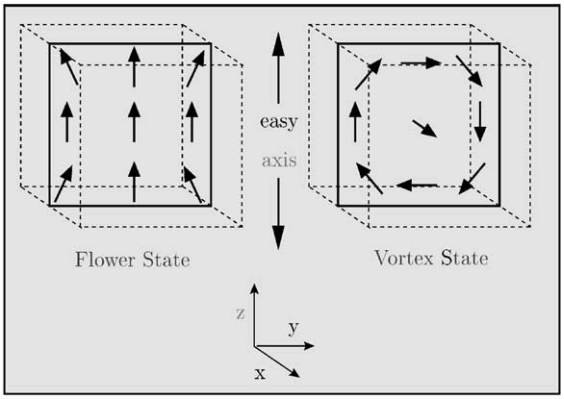

Fig. 1. Problem specification as first proposed by A. Hubert. The anisotropy parameter is chosen to be $Q = 0.1$.

Using reduced units, there is no need to explicitly define the material's parameters, i.e. the spontaneous polarization J_s, the magneto-crystalline anisotropy constant K and the exchange constant A. For this purpose the anisotropy parameter $Q = K/K_d$ is defined with the stray field constant $K_d = J_s^2/(2\mu_0)$. The size L of the cube is given in units of the exchange length $l_s = \sqrt{2\mu_0 A/J_s^2}$ and energies are expressed in reduced units, i.e. in units of $K_d V$ with $V = L^3$.

2. Micromagnetic algorithm

The magnetic structures and energies are calculated by means of numerical micromagnetic simulations with finite elements. The program is based on direct minimization of the total energy. In the following sections the basics of the algorithm are presented. More details about the code can be found elsewhere [3].

2.1. Discretization

We use five different meshes of tetrahedral finite elements to discretize the computational region (CR). The number of elements ranges from 35 822 in the case of the coarsest mesh to 100 283 elements in the mesh with the highest discretization density. To generate the grid, the CR is first subdivided into few tetrahedral elements using a Delaunay algorithm. Once a coarse mesh is defined, the elements are repeatedly bisected along their longest edge. This procedure generates finite elements with nearly uniform edge length and allows one to control both the total number of elements and the discretization density in selected areas of the CR to a certain extent. A minimum edge length l_{min} is defined as a stopping criterion for the bisectioning of elements. This minimum length is required for the edge of an element in order to be refined. The five meshes with different discretization density are generated by starting from one coarse mesh and applying the longest-edge-bisection method with different values of l_{min}. The smaller l_{min} is, the more elements are created. For details on this bisection method see Ref. [4].

The meshes with different discretization density are used to extrapolate the computed values, e.g. of the total energy, to the case of infinite discretization density. By doing so, errors resulting from the discrete representation of the vector fields involved in the calculation can be minimized. An example of this will be given in Section 4.2.

2.2. Energy terms

The equilibrium arrangement of the magnetic structure minimizes the Gibbs' free energy. Neglecting entropy, the problem is treated by minimizing the sum of the most important contributions to the total energy.

2.2.1. Exchange energy

The continuum representation of the exchange energy E_{exc} of a ferromagnet is given by

$$E_{\mathrm{exc}} = \int A \cdot \left[(\nabla m_x)^2 + (\nabla m_y)^2 + (\nabla m_z)^2\right] \mathrm{d}V, \quad (1)$$

where A is the exchange constant and $\boldsymbol{m} = (m_x, m_y, m_z)^{\mathrm{T}}$ is the unit vector of the local magnetization. In our code, the exchange energy for a given discretized distribution of magnetic moments is calculated by means of linear interpolation of the Cartesian components of the magnetization within each finite element. Hence, the exchange energy density is approximated as a piecewise constant function.

2.2.2. Magnetocrystalline anisotropy

The magnetocrystalline anisotropy energy in the case of uniaxial anisotropy writes

$$E_{\mathrm{an}} = \int K \sin^2\alpha \, \mathrm{d}V, \quad (2)$$

where α is the angle between the local magnetization and the easy axis. To calculate this term, the exchange energy density of the anisotropy is determined at the nodes (discretization points) and interpolated linearly within each element.

2.2.3. Stray field energy

The non-local nature of the stray field term causes difficulties in micromagnetic calculations. To reduce the numerical costs, the stray field and the stray field energy are not calculated directly. Instead, a variational approach is used which contains only local variables. The method is based on one of the two inequalities set up by Brown [5], who has shown that the stray field energy E_{st} and the induction $\boldsymbol{B}$ of a given distribution of magnetic moments $\boldsymbol{J}$ can be obtained by minimizing the functional on the right-hand side of the following equation with respect to $\boldsymbol{B}'$:

$$E_{\mathrm{st}} = \min_{\boldsymbol{B}'} \left\{ \frac{1}{2\mu_0} \int_{(\text{all space})} (\boldsymbol{B}' - \boldsymbol{J})^2 \, \mathrm{d}V \right\}, \quad (3)$$

with the constraint $\nabla \cdot \boldsymbol{B}' = 0$. Provided that $\boldsymbol{B}'$ is a solenoidal field, this term is minimized if and only if $\boldsymbol{B}'$ is equal to $\boldsymbol{B}$ in all space. Representing $\boldsymbol{B}'$ as the curl of a vector potential $\boldsymbol{A}$, the constraint of solenoidality is fulfilled automatically. In a numerical implementation, the term on the right-hand side of Eq. (3) can be calculated by means of an unconstrained minimization with respect to the set of Cartesian components of the discretized vector field $\boldsymbol{A}$ defined at the nodes.

The advantages of using this functional to calculate the stray field energy E_{st} are remarkable:

(1) Only local quantities are involved in the calculation of the stray field. The evaluation of a twofold integral is avoided.
(2) The minimization of functional (3) can be performed quickly. As the problem is convex, the functional behaves well and no problem concerning saddle-points needs to be considered.
(3) The memory requirements are low compared with other methods. No dense matrix is needed as is the case when boundary element methods are used [6,7].
(4) In this micromagnetic algorithm the dynamics of the magnetization is not considered. The magnetic structure is determined by direct minimization of the energy with respect to the direction of the magnetization at each node. This gives the possibility to calculate both the stray field and the minimum energy arrangement of the magnetization simultaneously [8]. By adding functional (3) to the exchange energy term and to the term of the magnetocrystalline anisotropy, the equilibrium arrangement of the magnetization can be

calculated by minimizing the resulting energy with respect to both the direction of the polarization and to the vector potential. This speeds up the calculation considerably as compared with an iterative calculation of the magnetic structure on one hand and the stray field on the other.

This method has—of course—some disadvantages, too. The drawback in this case is that the integral in Eq. (3) is extended over all space, including the non-magnetic area outside the sample. As numerical calculations with the finite element method necessarily consider only finite domains, some effort is needed to treat this open boundary problem where the integration is extended to infinity. Several techniques have been developed and successfully applied for such problems [7]. In our code the whole area outside the sample is mapped on a finite region by means of a bijective transformation. The "parallelepipedic shell transformation" [9] is applied. The sample is embedded between six non-magnetic segments as shown by Fig. 2. Each point inside these segments represents one point of the area outside the sample. The six segments are discretized into finite elements and are part of the CR.

By including the non-magnetic segments, the number of degrees of freedom is raised because the vector potential needs to be calculated in the surrounding segments, too. The previously mentioned benefits of this method, however, justify this additional numerical effort. The method presented here is based on an algorithm developed by Schrefl et al. [10]

The advantages of using finite elements in micromagnetism instead of finite differences are the capability to treat complex geometric

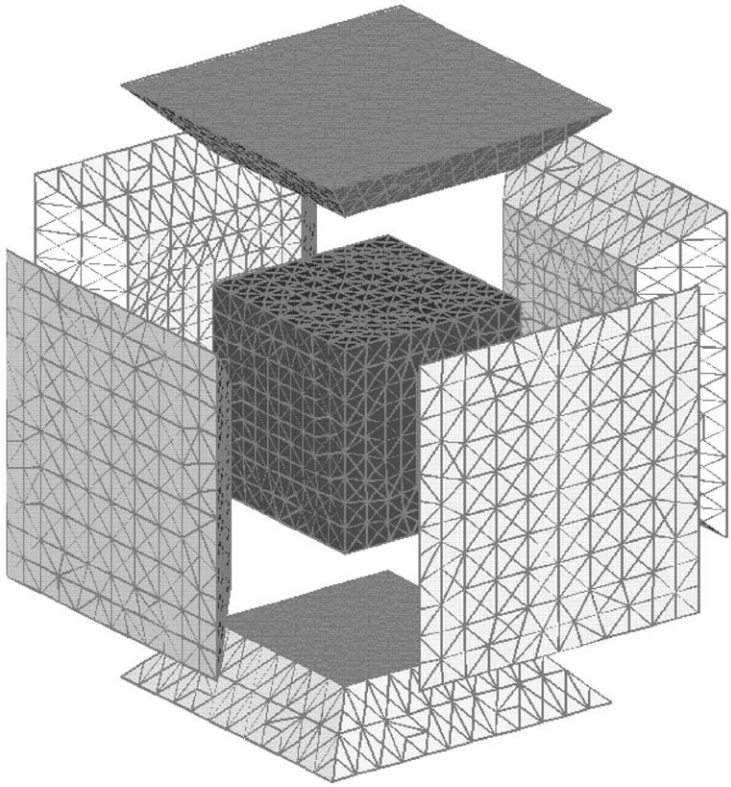

Fig. 2. Exploded view of the different domains considered in the CR. The unbounded area outside the ferromagnetic sample (cube in the middle) is mapped onto six finite domains surrounding the sample.

structures and to adaptively refine the discretization mesh in the case of large samples subdivided in domains. These advantages do not apply to Standard Problem No. 3, which is tailored to the finite difference method.

2.3. Energy minimization

As mentioned above, the energy is minimized directly, without taking into account the dynamics of the magnetization. The minimization of the total energy has to be performed under the constraint $|\boldsymbol{J}| = \text{const}$. This constraint can be enforced easily by representing the local polarization $\boldsymbol{J}_i$ at each node i with spherical coordinates:

$$\boldsymbol{J}_i = J \begin{pmatrix} \sin\vartheta_i \cos\varphi_i \\ \sin\vartheta_i \sin\varphi_i \\ \cos\vartheta_i \end{pmatrix}. \tag{4}$$

For a given initial configuration of $\boldsymbol{J}$ and random initial values for $\boldsymbol{A}$, term (3) is calculated first by minimization with respect to the discretized vector potential. After this, the sum of all energy terms is minimized with respect to the set of variables $\{\vartheta_i, \varphi_i, (A_x)_i, (A_y)_i, (A_z)_i\}$ defined at the nodes i. The minimization is performed with the conjugate gradient method [11], which has been proved to be very efficient in micromagnetic calculations [12].

Commercial minimization routines work very reliably. They can be tested with simplified models whose solutions are known. For instance, one may check whether an alignment of the magnetization parallel to an easy axis results if the stray field energy is switched off and a random initial configuration of the magnetization is chosen.

In the calculations presented here we use a stopping criterion (optimality tolerance parameter) of 10^{-12}, which is comparable to the machine's precision ($\simeq 10^{-16}$). This parameter is unnecessarily low [13]. It can be increased by five orders of magnitude without any relevant change of the result, i.e. in the first six significant digits of the calculated energy. This extremely low tolerance has been chosen to make sure that the stopping criterion does not have an influence on the result. The longer computation time resulting from this is not relevant for the calculation of the zero field states of the magnetization as the algorithm converges quickly.

3. Tests of the algorithm

Besides possible tests of the minimization routine as described above, the calculation of the single energy terms can be tested easily. The anisotropy term and the Zeeman term generally do not cause any problem and they can be tested by calculating these energy terms for a homogeneous magnetization which is tilted with respect to the easy axis or the external field. The stray field energy and the exchange energy require more subtle tests.

3.1. Stray field

As an example, the stray field and the stray field energy can be calculated for the case of a homogeneously magnetized cube. This is a suitable test to determine the discretization density required in the exterior region.

In Fig. 3, the field of the magnetic induction calculated for a homogeneously magnetized cube is displayed on a cross-section through the middle of the cube ($x = 0$). The transformation of the exterior region into the surrounding shell has been inverted for the visualization of the vector field so that the arrows outside the cube represent the induction in real space. It can be seen qualitatively that the boundary conditions (continuity of the normal component, jump condition of the tangential component) are fulfilled automatically.

The accuracy of the calculation of the stray field energy depends on the discretization density in the non-magnetic region outside the sample. As shown in Fig. 4, a good agreement with the analytical value is obtained quickly with increasing number of elements in the surrounding shell. According to this test of convergence, about 2×10^4 elements in the exterior region are used in the calculation of the magnetic structures. The five meshes used for the extrapolation of the data to the case of infinite discretization density differ only by the number of elements located in the interior magnetic region.

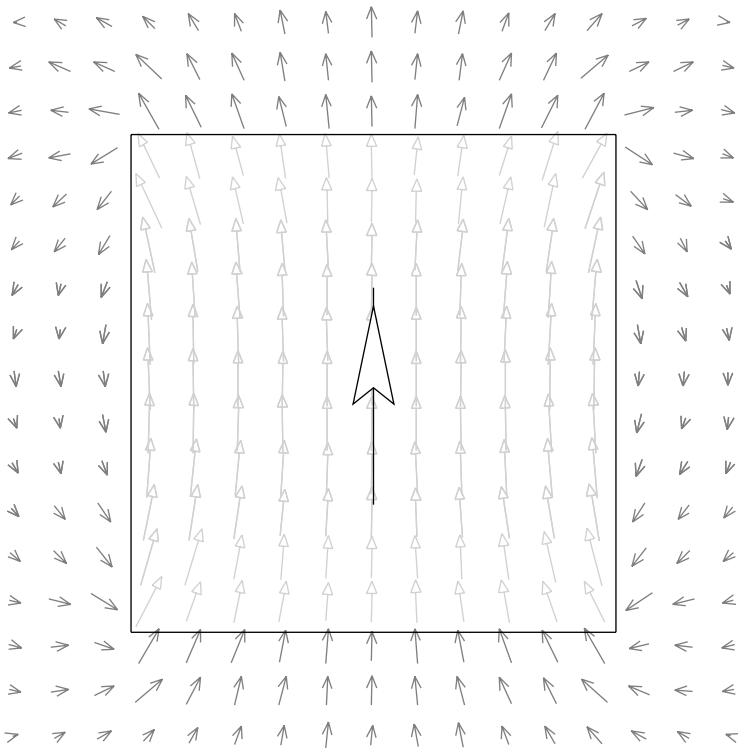

Fig. 3. Magnetic induction inside and outside the homogeneously magnetized cube. The big arrow indicates the direction of the magnetization. The location and the number of arrows is not related with the discretization points.

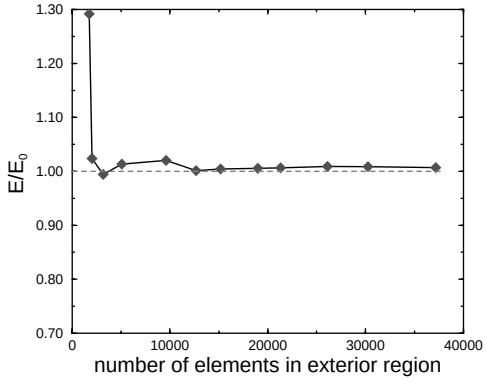

Fig. 4. Stray field energy in units of the analytical value $E_0 = K_d \cdot V/3$ as a function of the number of elements in the exterior region.

3.2. Exchange energy

The correctness of the calculation of the exchange energy term can be verified using a well-defined inhomogeneous arrangement of the magnetization whose exchange energy can be calculated analytically. For this purpose, a simplified form of a 180° wall is used as described in Fig. 5.

This magnetic structure yields a homogeneous exchange energy density and the analytic value of the total exchange energy is $E_{\mathrm{exc}}^{\mathrm{ideal}} = A\pi^2 L$. The ratio of the numerically obtained value to this analytical value as a function of the number of elements is shown in Fig. 6.

The exchange energy is systematically underestimated, as is expected due to the interpolation method. This effect is inherent in every discretization scheme. The finite element method allows for a precise approximation of the magnetic structure by means of a piecewise linear field, in contrast to the commonly applied methods which use piecewise homogeneous fields. The analytical value is approached very well with increasing discretization density. A global error significantly below 1% is obtained.

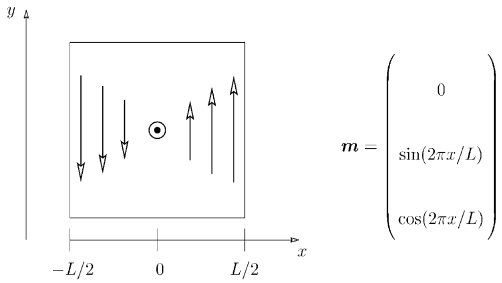

Fig. 5. Inhomogeneous arrangement used to test the calculation of the exchange energy.

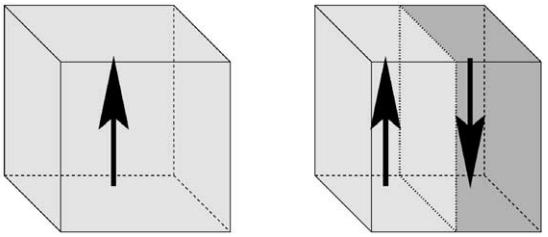

Fig. 7. Initial conditions of the calculation. The system is relaxed to an energetic minimum starting from both a homogeneous arrangement and a configuration subdivided into two domains.

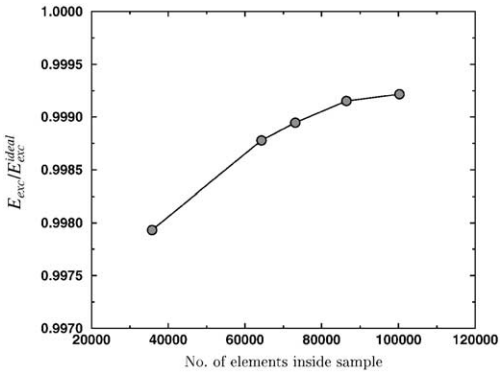

Fig. 6. Calculated exchange energy in units of the analytical (exact) value vs. number of finite elements used.

4. Details of the calculation

4.1. Initial conditions

Numerically as well as physically, it is not expected to find a ferromagnetic sample in the energetic ground state. There are generally several metastable structures at zero field. Which of these structures is realized depends only on the magnetic history of the sample. Therefore, it does not make much sense from a physical point of view to pinpoint the energetic ground state of the magnetization.

From a numerical point of view, however, it is important to have well-defined magnetization states if numerical results are to be compared. In this sense, the energetic ground state is a natural choice. To account for different possible magnetic histories, according to Fig. 7 two different initial configurations have been chosen in the calculation. The flower state is obtained by starting with a homogeneous magnetization parallel to the easy axis and the vortex state is calculated by starting with two antiparallel domains oriented in the easy axis direction.

These simple configurations are chosen to find homogeneous and inhomogeneous arrangements without prescribing the expected structures. In some cases, a breaking of symmetry may lead to energetically favored structures [3]. To facilitate this, the initial configurations are slightly perturbed prior to the energy minimization. The direction of the magnetization at each node is randomly perturbed with a magnitude of $\pm 1^\circ$. As will be shown below, this procedure is very important to find different remanent states.

4.2. Data extrapolation

The numerical values of the energy and the remanence of a magnetic structure obtained using a mesh of finite elements are always subjected to discretization errors. If analytical results are not available, it is difficult to state the quantitative effect of these errors. To determine results which are independent of the discretization, the calculations are performed with different meshes and the data are extrapolated to the case of infinite discretization density. An example for this is shown in Fig. 8. When plotted over N^{-1}, an almost linear dependence is found for the energy terms and for the remanence (N is the total

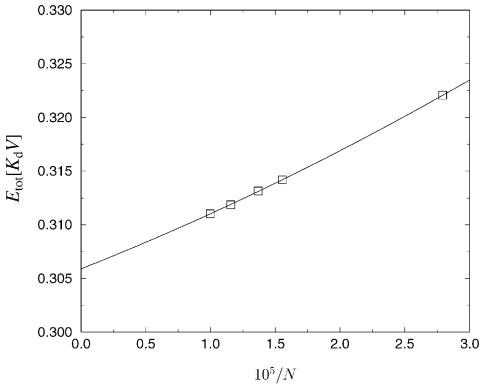

Fig. 8. Total energy of the vortex state at $L = 8.5 \cdot l_s$ obtained using different discretization densities. The values are extrapolated to the case $N \to \infty$.

number of elements). By means of a least-square fit, a second-order polynomial function is determined with which one can extrapolate the results convincingly to infinite discretization density, i.e. $N^{-1} \to 0$.

This extrapolation procedure may seem questionable because the continuum description of micromagnetism is not valid on length scales significantly below the exchange length. Hence, when the cell size is very small, an atomistic treatment is required to describe the magnetic structure in the area enclosed by the element. However, it should be kept in mind that the discretization merely determines the quality of the numerical representation of the continuum approximation. As we are only interested in a micromagnetic description, there is no inconsistency in extrapolating to infinitely small cell sizes.

5. Results

5.1. Flower state

When starting from the homogeneous arrangement at small edge lengths, the expected Flower state results as shown in Fig. 9. This magnetic structure is mostly homogeneous. Only in the vicinity of the edges and corners the magnetization spreads outside due to the inhomogeneity of the stray field. The magnetization tends to align

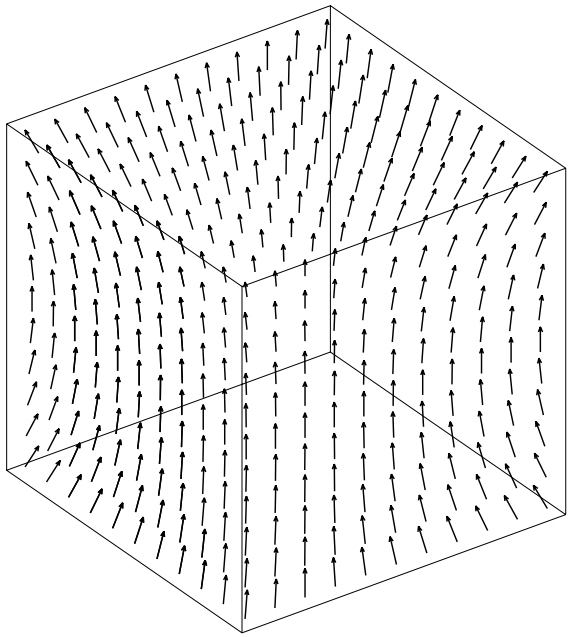

Fig. 9. Three-dimensional representation of the flower state. The magnetization is mainly homogeneous and oriented parallel to the easy axis.

parallel to the local induction which is similarly tilted near the edges, see Fig. 3. This tilting has been found by Schabes and Bertram [14] and has been studied, e.g., by Schmidts and Kronmüller [15], by Rave et al. [16] and by Usov and Peschany [17].

According to the problem specification, the size dependence of the energy of this structure has to be determined and compared with the vortex state, which will be discussed in Section 5.3.

5.2. Twisted flower state

Increasing the size of the sample, the flower state becomes energetically unstable. A spontaneous collapse is observed at an edge length of about $L \simeq 8.6 \cdot l_s$. At sizes above this edge length, a different magnetic structure results which we have named twisted flower state. As a characteristic effect, the remanence in the easy axis direction —when plotted as a function of the edge length—is suddenly reduced once the ordinary flower state converts into the twisted flower state, see Fig. 10. The magnetic structure of the twisted

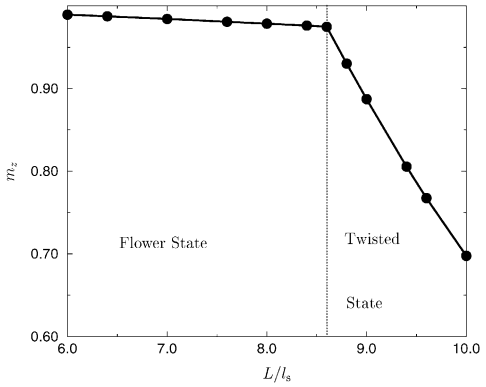

Fig. 10. Collapse of the flower state with increasing size. The sudden change of the remanence in the easy axis direction m_z indicates the conversion of the flower states into the twisted flower state.

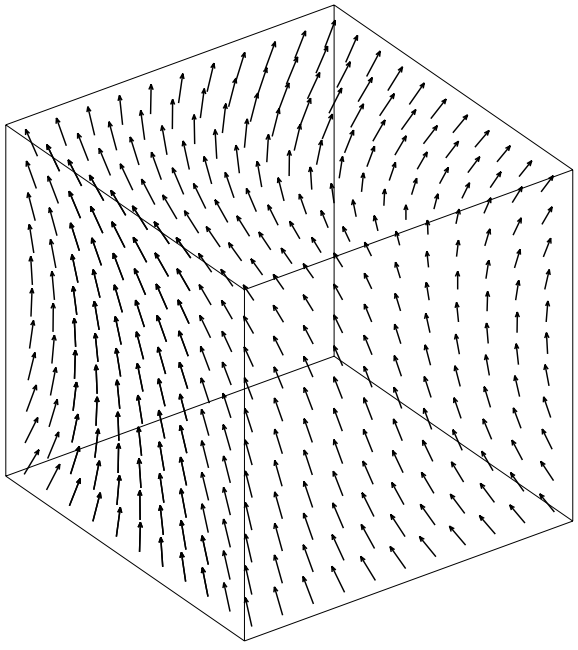

Fig. 11. Magnetic structure of the twisted flower state.

flower state is shown in Fig. 11. Similar to the flower state, the homogeneity of the arrangement is mostly preserved. The qualitative difference to the flower state is a twist of the magnetization along the easy axis. This can be readily seen in the cross-sections of this arrangement shown in Fig. 12. In an interesting fashion, this arrangement endorses the tendency to maintain a homogeneous state parallel to the easy axis on one hand and to reduce the stray field energy on the other by forming a structure similar to a vortex.

Several names could be found to describe this structure. The similarity to the magnetization reversal mode of infinitely extended cylinders known as curling would justify the name "curled state" [18,19]. The twisted flower state has been reported first by Schabes and Bertram [14], who called this structure a "vortex state". Indeed, if the size of the cube is further increased, the twisted flower state modifies continuously such as to form a longitudinal vortex state, i.e. a vortex structure with its axis parallel to the easy axis. As there are no closed flux lines inside the sample at the edge lengths considered here, we have dismissed this term. The term twisted flower state has been chosen as we interpret this structure with its high remanence to be a modified version of the flower state described previously.

To calculate the twisted flower state, no special starting conditions need to be chosen. The structure may develop automatically by simply using a homogeneous initial configuration. However, since the symmetry needs to be broken, the previously mentioned small random perturbation of the starting configuration is essential for obtaining the twisted flower state. Correspondingly, the edge length at which the flower state collapses shown in Fig. 10 is not a critical edge length at which the transition occurs but simply a size at which the stability of the flower state is reduced sufficiently for random perturbations to lead to a different structure. The edge length at which the flower state collapses depends on the magnitude of the perturbations. Therefore, the size dependence of the energy of the twisted flower state is studied by reducing the size of the cube after the flower state has collapsed.

The results indicate that, for $Q = 0.1$, if both structures are possible, the twisted flower state has a lower energy than the flower state. However, the twisted flower state is not found in very small cubes. The characteristic twist hardly develops in smaller cubes, so that in very small cubes a distinction between these homogeneous states becomes needless since the twisted flower state

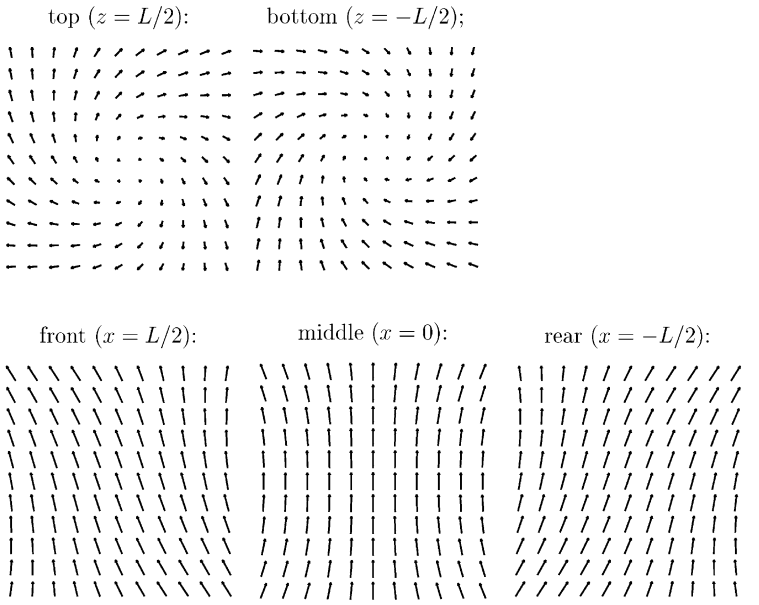

Fig. 12. Twisted flower state, projection of the magnetization on different planes. The twist of the magnetization is clearly recognizable when looking on a plane with $z = \text{const}$.

converts into the "ordinary" flower state. There seems to be a second-order phase transition between the flower state and the twisted flower state at an edge length of about $8.0 \cdot l_s$ which we have not investigated in detail.

5.3. Vortex state

The magnetic structure of the vortex state is shown in Fig. 13 and on the cross-sections in Fig. 14. A small x-dependence of the magnetic structure is observed. The magnetization on the front side ($x = L/2$) and on the back side ($x = -L/2$) differs from the magnetic structure in the middle ($x = 0$). Similar to the twisted flower state (see Fig. 12, $z = \pm L/2$), the vortex on the front side has a radial component directed outside the sample while on the back side a small radial component can be seen which is directed towards the core of the vortex. In the middle plane $x = 0$ the vortex is symmetric but elongated in the easy axis direction. In another cross-section through the middle of the sample ($z = 0$) shown on the lower right of Fig. 14 the Bloch line can be seen clearly. On the vortex axis, i.e. the x-axis, the magnetization is perpendicular to the vortex plane.

5.4. Vortex state with singularity

A topologically interesting modification of the vortex state has been found which contains a micromagnetic singularity. This type of singularity is sometimes called Feldtkeller singularity [20] or Bloch point [21]. Cross-sections through the sample at $x = 0$, $y = 0$ and $z = 0$ for this structure are shown in Fig. 15.

The gray scaling in Fig. 15 represents the z-component of the magnetization on the cut at $x = 0$ and the x-component on the other two cuts.

The main difference between this type of vortex structure and the ordinary vortex structure can be seen in the Bloch line which is interrupted by the singularity. Following the Bloch line on the x-axis, the magnetization changes its direction at one point in the middle of the sample. On the surfaces, the magnetization in the middle of the vortex is oriented outside the sample on both sides while in the case of the ordinary vortex state it is directed

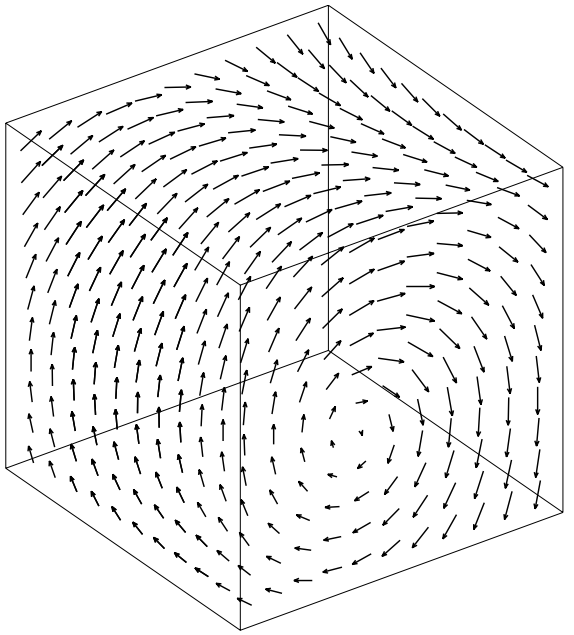

Fig. 13. Vortex state. This structure is obtained using two domains with antiparallel magnetization as starting conditions.

inside the sample on one side and outside the sample on the opposite side. The vortex structure with singularity is *completely* demagnetized, i.e. the remanence vanishes in every direction.

In the close vicinity of the singularity any direction of the magnetization can be found. Hence, the ferromagnetic order of the material breaks down at this point and the magnetization changes its direction by 180° on an atomistic level. No direction of the magnetization can be defined at the singularity.

While the existence of such singularities is well known and the magnetic structure near these points has been studied in detail by means of analytic approaches [22,23], micromagnetic simulations on these structures have not been found in the literature.

The profiles of the Bloch line, which are recognizable from the gray scaling in the $y = 0$ and in the $z = 0$ cut in Fig. 15, are in good agreement with those predicted by analytical calculations [24,25].

In order to analyze this structure in the close vicinity of the singularity an atomistic description is desirable as proposed previously [26]. The micromagnetic equations—especially the exchange energy term—are not suitable to describe the singularity reliably. Nevertheless, the error resulting from the micromagnetic numerical calculation affects only a very small volume and the global error can be deemed low. A large error occurs especially in the one element which contains the singularity. If the discretization is sufficiently high, the error resulting from this small element should be negligible. It is not expected that this error significantly influences the result for the overall magnetic structure on a larger length scale.

This vortex structure with a singularity represents a further stable state of the magnetization which can be found in the ferromagnetic cube specified in Standard Problem No. 3. The stability of this structure can be understood easily. Any displacement of the singularity from the center increases the remanence and hence increases the stray field energy of the system while no significant change of the other energy terms is expected. If the singularity is shifted to the surface along the x-axis the structure converts into the ordinary vortex state. An energetic barrier has to be overcome by applying an external field to bring the singularity to the surface. In this case, the singularity becomes a singular point (swirl) and the high exchange energy near the singularity is released.

5.5. Size dependence of the magnetic ground state

The evaluation of the total energies of the flower state, the twisted flower state and the vortex state for different edge lengths yields the diagram shown in Fig. 16.

The critical edge length at which the magnetic ground state changes from the twisted flower state to the vortex state is at $8.57 \cdot l_s$. At this edge length we find that the twisted flower state and the vortex state have the same total energy E_{tot}. This is considered to be the SDL of the cube analyzed here. The partial energies and the mean reduced magnetization for this critical edge length are displayed in Table 1.

We find a SDL which is qualitatively different from the one according to the problem specification, where a transition between the flower state

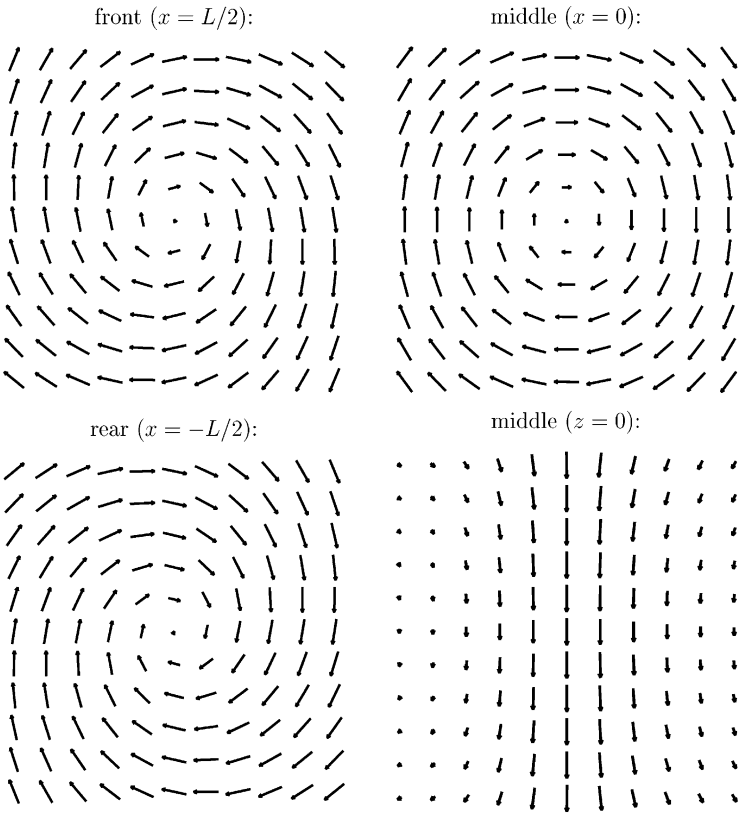

Fig. 14. Vortex state, projection of the magnetization onto different cross-sections.

and the vortex state was expected. For reasons of comparison between our results and those submitted by other groups, we also calculated the edge length at which the flower state and the vortex state degenerate energetically. This edge length was determined to $L = 8.52 \cdot l_s$. The results for this transition are summarized in Table 2.

The total energy of the vortex state with singularity is relatively high compared with the other configurations. This magnetization state does not represent a magnetic ground state due to its high exchange energy. This holds for the range of size considered in this paper. As an example, the energy terms of this magnetization state at the edge length $L = 8.50 \cdot l_s$ are listed in Table 3. At a significantly larger edge length the vortex state with singularity is likely to yield a lower energy than the (ordinary) vortex state because of the very low stray field energy of this completely demagnetized structure.

6. Discussion

The calculation of the SDL of the ferromagnetic cube according to Standard Problem No. 3 has yielded an unexpected transition of magnetic ground states with increasing size. In the relevant range of sizes, the flower state does not represent a magnetic ground state. The twisted flower state has a lower energy than the flower state. Calculations performed by W. Rave after we submitted our results to the μMAG group are in agreement with this. As an impact of these results on Standard Problem No. 3 we suggest the transition from the twisted flower state to the vortex state in further submissions.

6.1. Comparison with other groups

Currently, three solutions to Standard Problem No. 3 are available [2]. The results of Rave et al.

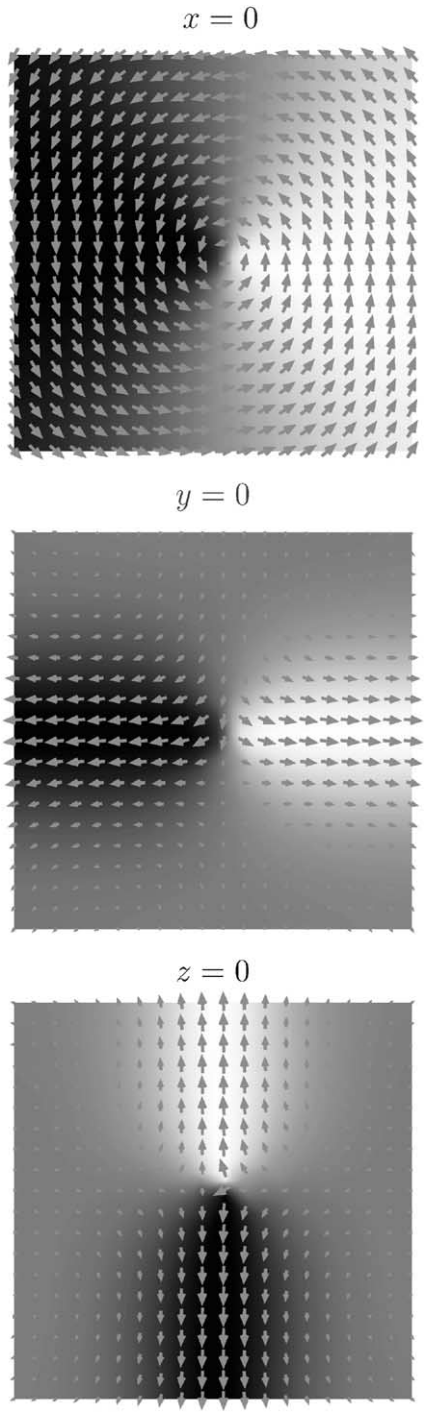

Fig. 15. Vortex state with singularity. The singularity is located in the middle of the sample. No direction of the magnetization can be assigned to this point.

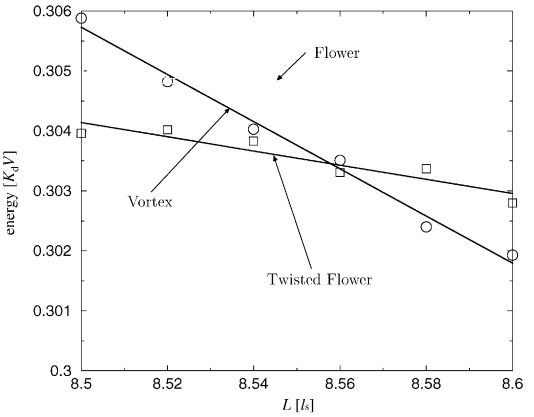

Fig. 16. Size dependence of the total energy of different magnetization states in the ferromagnetic cube of Standard Problem No. 3.

Table 1
Critical edge length, total energy and partial energies in units of $K_d \cdot V$ of the twisted flower state and the vortex state at the critical edge length (SDL). The non-vanishing components of the remanence are listed for these structures at the SDL

Twisted flower state $\leftrightarrow$ vortex state		
$L = 8.56 \cdot l_s$,	$E_{tot} = 0.3034 \cdot K_d V$	
	Twisted flower state	Vortex state
Stray field	0.2337	0.0820
Exchange	0.0464	0.1693
Anisotropy	0.0232	0.0521

Twisted flower: $\langle m_z \rangle = 0.875$.
Vortex: $\langle m_y \rangle = 0.345$.

Table 2
Data on the transition between flower state and vortex state as listed in Table 1

Flower state $\leftrightarrow$ vortex state		
$L = 8.52 \cdot l_s$,	$E_{tot} = 0.3049 \cdot K_d V$	
	Flower state	Vortex state
Stray field	0.2839	0.0830
Exchange	0.0158	0.1696
Anisotropy	0.0052	0.0522

Flower: $\langle m_z \rangle = 0.973$.
Vortex: $\langle m_y \rangle = 0.351$.

Table 3
Partial energies of the vortex state with singularity at the edge length $L = 8.50 \cdot l_s$. The total energy of this configuration is higher than it is in the vortex state, but it is of the same order of magnitude

Vortex state with singularity	
	Energy $[K_d \cdot V]$
Stray field	0.0602
Exchange	0.2469
Anisotropy	0.0476
Total	0.3548

[16] are in perfect agreement with those by Ribeiro et al. These groups did not report the twisted flower state and determined the edge length at which the flower state and the vortex state have the same energy.

This "critical" edge length differs in our solution by 0.6% from these results and the energy of these arrangements at this edge length differs by 0.7%. Considering that the calculations presented here have been performed using a totally different method, we obtain a very good agreement. The code used by Ribeiro et al. seems to be very similar to the one used by Rave et al. (evaluation of the stray field using FFT, finite differences), so that the excellent agreement of these two groups might be less informative.

6.2. Possible errors

We suggest the following reasons as possible sources for the minor differences between our results and those submitted previously:

(1) The precision of the calculation of the stray field energy in our code is limited by the approximations due to the shell transformation of the exterior region. The discretization of the exterior region has been kept constant for all meshes. An extrapolation to infinity of the discretization density in the surrounding shells might lead to slightly different results.
(2) The calculation of the stray field energy by means of a vector potential is indirect and less precise than with a scalar potential. In demagnetized states the magnetic induction $\boldsymbol{B}$ is essentially equal to the polarization $\boldsymbol{J}$ so that small errors in the calculation of $\boldsymbol{B}$ might lead to significant errors when the term $(\boldsymbol{B} - \boldsymbol{J})$ is evaluated, see Eq. (3).
(3) Due to the irregular shape and orientation of the finite elements, any artificial anisotropy resulting from the numerical representation of the exchange energy is averaged out. It would be interesting to analyze whether this also holds for finite difference representations. In this regard, it would be illustrative to check whether the number of neighboring discretization cells considered in the calculation of the exchange energy of three-dimensional structures has an influence on the result. For two-dimensional systems a similar study has been performed by Donahue et al. [27].

References

[1] R.D. McMichael, M.J. Donahue, J. Appl. Phys. 81 (8) (1997) 5242.
[2] R.D. McMichael, Standard Problem Number 3, Problem Specification and Reported Solutions, Micromagnetic Modeling Activity Group, http://www.ctcms.nist.gov/~rdm/mumag.html, 1998.
[3] R. Hertel, H. Kronmüller, Phys. Rev. B 60 (10) (1999) 7366.
[4] R. Hertel, H. Kronmüller, IEEE Trans. Magn. 34 (6) (1998) 3922.
[5] W.F. Brown Jr., J. Phys. Soc. Jpn. 17 (Suppl. B-I) (1962) 540.
[6] D.R. Fredkin, T.R. Koehler, IEEE Trans. Magn. 26 (2) (1990) 415.
[7] Q. Chen, IEEE Trans. Magn. 33 (1) (1997) 663.
[8] P. Asselin, A.A. Thiele, IEEE Trans. Magn. 22 (6) (1986) 1876.
[9] X. Brunotte, G. Meunier, J.F. Imhoff, IEEE Trans. Magn. 28 (2) (1992) 1663.
[10] T. Schrefl, J. Fidler, H. Kronmüller, J. Magn. Magn. Mater. 138 (1994) 15.
[11] NAG-FORTRAN library programs, Numerical Algorithms Group, Ltd., Oxford, 1990.
[12] L. Lopez-Diaz, J. Eicke, E. Della Torre, IEEE Trans. Magn. 35 (3) (1999) 1207.
[13] W.H. Press, B.P. Flannery, S.A. Teukolsky, W.T. Vetterling, Numerical Recipies: The art of scientific computing, Cambrige University Press, Cambridge, New York, 1986.
[14] M.E. Schabes, H.N. Bertram, J. Appl. Phys. 64 (3) (1988) 1347.

[15] H.F. Schmidts, H. Kronmüller, J. Magn. Magn. Mater. 94 (1991) 220.
[16] W. Rave, K. Fabian, A. Hubert, J. Magn. Magn. Mater. 190 (1998) 332.
[17] N.A. Usov, S.E. Peschany, J. Magn. Magn. Mater. 135 (1–3) (1994) 111.
[18] A.J. Newell, R.T. Merrill, J. Appl. Phys. 84 (8) (1998) 4394.
[19] A. Aharoni, J. Appl. Phys. 86 (2) (1999) 1041.
[20] E. Feldtkeller, Z. Angew. Phy. 19 (1965) 530.
[21] J.C. Slonczewski, AIP Conf. Proc. 24 (1975) 613.
[22] W. Döring, J. Appl. Phys. 39 (1968) 1006.
[23] A. Aharoni, J. Appl. Phys. 51 (1980) 3330.
[24] A. Hubert, J. Magn. Magn. Mater. 2 (1976) 25.
[25] A.H. Eschenfelder, Magnetic Bubble Technology, Springer Series in Solid-State Sciences, Springer, Berlin, Heidelberg, New York, 1980.
[26] H. Kronmüller, R. Fischer, R. Hertel, T. Leineweber, J. Magn. Magn. Mater. 175 (1997) 177.
[27] M.J. Donahue, R.D. McMichael, Physica B 233 (4) (1997) 272.